

***Eupatorium Adenophora* (Spreng.) leaves Extract as a Highly Efficient Eco-friendly Inhibitor for Steel Corrosion in trichloroacetic acid Solution**

Gaofei Wei^{1,2}, Shuduan Deng³, Xianghong Li^{1,2*}

¹ Key Laboratory of State Forestry and Grassland Administration on Highly-Efficient Utilization of Forestry Biomass Resources in Southwest China, Southwest Forestry University, Kunming 650224, P.R. China;

² College of Chemical Engineering, Southwest Forestry University, Kunming 650224, P.R. China

³ Faculty of Materials Science and Engineering, Southwest Forestry University, Kunming 650224, P.R. China

*E-mail: xianghong-li@163.com

Received: 3 September 2022 / Accepted: 4 October 2022 / Published: 20 October 2022

Eupatorium Adenophora (Spreng.) leaves extract (EASLE) was prepared by using reflux method with the ethanol aqueous water solution as the extraction agent. The inhibition effect of EASLE on cold rolled steel (CRS) in 0.10 M Cl₃CCOOH solution was studied by weight-loss method, potentiodynamic polarization curves (PDP) and electrochemical impedance spectroscopy (EIS). The morphology of CRS surface was observed by scanning electron microscopy (SEM) and atomic force microscopy (AFM). The chemical composition of adsorbed film on CRS surface was characterized by X-ray photoelectron spectroscopy (XPS). The results show that EASLE exhibits a significant inhibitive performance for CRS in 0.10 M Cl₃CCOOH medium, and the maximum inhibition efficiency of 100 mg L⁻¹ EASLE at 15°C is up to 91.1%. EASLE adsorbs on CRS surface by exothermic adsorption, and conforms to Langmuir isotherm. PDP indicate that EASLE is a mixed-type inhibitor, and its electrochemical mechanism is through "geometric blocking effect". After adding EASLE, the charge transfer resistance is increased significantly, but the constant phase element decreased to some extent. SEM and AFM images clearly indicate EASLE can efficiently retard the corrosion of CRS surface by Cl₃CCOOH media. XPS analysis confirms that EASLE molecules adsorbed on CRS surfaces.

Keywords: inhibition; steel; *Eupatorium Adenophora* (Spreng.); trichloroacetic acid; adsorption

1. INTRODUCTION

Metallic materials play an extremely important role in the chemical industry. The properties of metals will gradually be deteriorated over time owing to corrosion. At the same time, the service-life of metal devices and equipment will be shortened. Corrosion problems will not only cause huge

economic losses, but also bring about serious safety hazards and safety accidents. It is estimated that China's economic losses caused by corrosion was about 2127.8 billion RMB in 2014, accounting for 3.34% of GDP [1]. Unlike the natural disasters, the metallic corrosion can be efficiently controlled and prevented by taking proper anti-corrosive measures. There are many common methods to retard or alleviate corrosion, among which adding inhibitor is one of the most efficient ways to protect metal materials in the chemical engineering field. Most corrosion inhibitors are organic compounds containing N, O, S, and (or) P atoms, polar functional groups (-OH, -NH₂, C=O, C-O, C-N), and (or) double bonds as well as hetero aromatic rings. In view of chemical structures, these compounds always have abundant lone-pair electrons, which can easily coordinate with unoccupied orbitals of metallic atom to adsorb on metal surface to form a protective barrier, and thus achieving the purpose of slowing down metallic corrosion [2].

Along with the enhancement of green development concept, the research and development of cheap, biodegradable and environment-friendly inhibitors has been paid more and more attentions all over the world. In the application of corrosion inhibitors, plant extract as a kind of natural products has some outstanding advantages, such as non-toxic, pollution-free, low cost, high efficiency and rich natural resources [3-5]. Especially in the 21st Century, more and more plant extracts have been reported as efficient inhibitors to retard the corrosion of steel in acid medium, the examples are listed as follows: black pepper [6], henna [7,8], *Justicia gendarussa* [9], *Strychnos nux-vomica* [10], *Artemisia pallens* [11, 12], *Punica granatum* [13], *Neolamarckia cadamba* [14], *Pennisetum* [15], thyme [16], *Myristica* [17], coffee [18], *Geissospermum* leave [19], *Damsissa* [20], fruit peel [21], *Ananas comosus* [22], *Musa paradisiaca* [23], *Nypa fruticans* Wurmb [24], *Tagetes erecta* [25], *Occimum viridis* [26, 27], *Kopsia Singapurenis* [28] and *Zenthoxylum alatum* [29]. These results showed that the main inhibitory substances in plant extracts include glycosides, alkaloids, flavonoids, phytosterol, saponins steroids, tannins, phlobatannins, anthraquinones, aminoacids, triterpenes and phenolic compounds [30]. These phytochemicals contain polar functional groups like hydroxyl (-OH), amino (-NH₂), amide (-CONH₂), acid chloride (-COCl), carboxylic acid (-COOH) and ester (-COOC₂H₅), which easily interact with metal and adsorb on metal surface to form films, which can achieve the purpose of inhibiting metallic corrosion [31-33]. Since then, our research group systematically studied inhibition performance of plant extracts on CRS in inorganic acids (HCl, H₂SO₄, H₃PO₄) solutions, for instance bamboo leaves [34,35], *Jasminum nudiflorum* Lindl. [36], *Mikania micrantha* [37], walnut green husk [38] and *ginkgo biloba* leaves [39]. In view of these published literatures, the plant extract has a good prospect for industrial application. However, the active components and inhibition mechanism of plant inhibitors are still rather difficult to be clarified. Moreover, there is little report about plant extracts as the corrosion inhibitor in organic acid media.

Trichloroacetic acid (Cl₃CCOOH) can be used as a common pickling preparation for metal surfaces to remove the oxide and rust layer on the surface of metal materials. In addition, Cl₃CCOOH is widely used in the cellulose industry, metallic equipment will be corroded in these processes of production and transportation. The electron-withdrawing effect of the three chlorine atoms makes Cl₃CCOOH more acidic ($K_a^{\circ}=0.22$). Accordingly, Cl₃CCOOH has a devastating corrosive on metallic surface, and then inhibitors are needed to be added to Cl₃CCOOH medium so as to protect the metallic substrate. As early as 1974, Sampat and Vora [40] studied methyl pyridines as an inhibitor on

aluminium for Cl_3CCOOH . The results showed that N atom was the key adsorption site on the metal surface, and the introduction of methyl on pyridine ring increased the inhibition effect due to specific adsorption effect, the inhibition performance followed the order: nicotine > 2,6-lutidine > 2,4-lutidine > α -picoline > β -picoline > piperidine > pyridine. Amino acetanilide [41], xylenol orange [42], sulfathiazole [43] and 2-acetophenthiazine [44] have been reported as effective inhibitors for aluminum in Cl_3CCOOH medium in the 21st century. However, after a careful review of the published literatures, there is little report on steel in Cl_3CCOOH medium. Therefore, it is urgent to screen out the effective inhibitor with low cost and environment friendly in Cl_3CCOOH medium.

Our work-team has been doing some researches about the corrosion inhibitors for steel in Cl_3CCOOH solution. Anionic surfactants of calcium lignosulfonate [45] and sodium dodecyl sulfate [46], as well as N-heterocyclic compounds of imidazoline [47] and triazolyl blue tetrazolium bromide [48] were found to behave as effective inhibitors for steel in Cl_3CCOOH medium. Besides the organic compounds, bamboo leaves extract [49] was tested as inhibitor of steel in Cl_3CCOOH medium, and its maximum inhibition efficiency was 96.1% with 200 mg L^{-1} at 20°C . Recently, it is found that there is a synergistic inhibition effect of walnut green husk extract with KI for steel in Cl_3CCOOH solution [50]. These results implies that it would be an efficient pathway to seek an efficient inhibitor from the plant extract.

Eupatorium Adenophora (Spreng.) (EAS) is a highly alien invasive species in China [51,52]. It is extremely adaptable [53] in drought, barren slopes, and even rock crevices and rooftops, which and can spread rapidly with its powerful roots. Once it is invaded, it will quickly form a single dominant species community, and compete with the original plants for water, fertilizer, light and space, then disrupt biodiversity and disrupting the local ecological balance [54]. In order to prevent and control EAS invasion, various measurements are put forward, such as manual and mechanical control and chemical control. The main chemical components of EAS are flavonoids, phenylpropanoids, phenols, steroids, polysaccharides and other compounds [55]. These compounds have a large number of polar groups containing O atoms (hydroxyl group, carbonyl group, ether bond, O-heterocyclic ring), aromatic groups, unsaturated double bond and conjugated structure in their molecular structures, which may be a potential corrosion inhibitor. Thus, our work-team develop a novel idea that EAS is extracted to be the inhibitor to prevent the metallic corrosion, which can promote the comprehensive utilization of EAS resources, and then achieve the purpose of "turning waste into treasure".

In this study, the inhibition effect of EASLE on CRS in Cl_3CCOOH medium is firstly investigated by weight-loss method, potentiodynamic polarization curves (PDP) and electrochemical impedance spectroscopy (EIS). The influence of temperature and inhibitor concentration on the inhibitive action are fully investigated. Scanning electron microscopy (SEM) and atomic force microscopy (AFM) were used to characterize the microstructure of CRS surface. X-ray photoelectron spectroscopy (XPS) was used to analyze the chemical compositions of the adsorption layer on CRS surface in the presence of inhibitor. It is expected to provide a theoretical basis for exploring the inhibition mechanism of EASLE on CRS in Cl_3CCOOH medium.

2. EXPERIMENTAL

2.1. Materials

CRS samples were obtained from Panzhihua steel plant. CRS is composed of 0.07% C, 0.3% Mn, 0.022% P, 0.010% S, 0.01% Si, 0.030% Al and the remaining Fe. Trichloroacetic acid (Cl_3CCOOH), anhydrous ethanol, acetone and petroleum ether are analytical pure reagents.

2.2. Preparation of EASLE and FTIR

The fresh leaves of EAS were collected, washed and air-dried at room temperature, and put into an oven to be completely dried at 50°C , then crushed to obtain EAS leaves powder. The raw materials powder (10 g) was immersed in 250 mL of 40% (volume fraction) ethanol aqueous solution for 2 h at room temperature, and then refluxed at 75°C for 2 h. The concentrated solution was extracted by rotary evaporation with petroleum ether, and then put into the surface dish. Finally, about 1.2 g of brown solid EASLE was obtained by vacuum drying (the extraction rate was about 12%).

The functional groups of EASLE were measured by Avatar-FTIR-360 infrared spectrometer (Thermo Nicolet, USA) using KBr pressed-disk technique, and the wavenumbers range was $250\text{-}4000\text{ cm}^{-1}$.

2.3. Weight loss measurements

CRS sheet was cut into $25\text{ mm} \times 20\text{ mm} \times 0.5\text{ mm}$ sample, and the whole surface was polished step by step with a series of emery papers (grade 120-600-1500), and cleaned with distilled water, then degreased with acetone. After weighing by a digital balance with a sensitivity of $\pm 0.1\text{ mg}$, the steel sheets were totally immersed in 250 mL Cl_3CCOOH solution nonexistence and existence $10\text{-}100\text{ mg L}^{-1}$ EASLE for 6 h at different temperatures controlled by a water bath. The specimens were taken out, rinsed under running water with a bristle brush to get rid of corrosion products, blow dried in cold air, and reweighed accurately. The corrosion rate (v) is calculated according to Eq. (1), and then inhibition efficiency from weight loss (η_w) is obtained according to Eq. (2).

$$v = \frac{W}{St} \quad (1)$$

where W is the average weight loss of three parallel CRS sheets (g), S the total area of one CRS specimen (m^2), and t is the immersion time (h).

$$\eta_w = \frac{v_0 - v}{v_0} \times 100\% \quad (2)$$

where, v_0 and v are the values of corrosion rate without and with inhibitor, respectively.

2.4. Electrochemical measurements

PDP and EIS measurements were performed using a conventional three-electrode system on PARSTAT 2273 advanced electrochemical system (Princeton Applied Research). The reference electrode is a Luggin capillary coupled with the saturated KCl calomel electrode (SCE), the counter electrode is platinum electrode (Pt261), and the working electrode (WE) is CRS sheet. WE is encapsulation with epoxy resin (curing agent is polyamide resin). Its exposed surface (1.0 cm × 1.0 cm) was treated in Sec. 2.3, and was put into an electrolytes cell containing 250 mL 0.10 M Cl₃CCOOH solution in the absence and presence of different concentrations of EASLE. After immersion in test solution at OCP for 2 h to stabilize the system, the electrochemical test was performed. PDP curves was measured at scan interval of -250 ~ +250 mV versus OCP and scan rate of 0.5 mV s⁻¹. The inhibition efficiency of PDP (η_p) can be calculated through Eq. (3) [56]:

$$\eta_p = \frac{i_{corr} - i_{corr(inh)}}{i_{corr}} \times 100\% \quad (3)$$

where $i_{corr(0)}$ and $i_{corr(inh)}$ represent corrosion current densities in the absence and presence of EASLE, respectively.

The frequency range of EIS measurement is 0.01 ~ 10⁵ Hz, and the AC excitation amplitude is set as 10 mV. The inhibition efficiency from EIS (η_R) is calculated by following Eq. (4) [57].

$$\eta_R = \frac{R_p(inh) - R_p(0)}{R_p(inh)} \times 100\% \quad (4)$$

where $R_p(0)$ and $R_p(inh)$ are polarization resistance values in the absence and presence of EASLE, respectively.

2.6. Characterization of CRS surfaces

The CRS sample of 25 mm × 20 mm × 0.5 mm was prepared according to Sec. 2.3. Under the condition of 15°C, the samples were immersed in 0.10 M Cl₃CCOOH solutions nonexistence and existence 100 mg L⁻¹ EASLE for 6 h, and taken out and scrubbed with cotton under running water, blow dried in cold air, then used for surface characterizations. Japan instrument model S-3000N scanning electron microscope (Hitachi High-Tech Science Systems Corporation) was used for SEM experiments. AFM examinations were carried on a Japan instrument model SPA-400 SPM Unit atomic force microscope with the tapping mode using Si₃N₄ tips. XPS were done by K-Alpha photoelectron spectrometer (Thermo Fisher Scientific, USA) with Al K alph radiation ($h\nu = 1486.8$ eV).

3. RESULTS AND DISCUSSION

3.1. FTIR of EASLE

Fig. 2 shows FTIR spectra of EASLE. The absorption peaks shown in the figure are assigned as follows: the strong absorption peak at 3384 cm⁻¹ is N-H or O-H stretching vibration of carboxyl group (-COOH), phenolic hydroxyl group (-OH) and -NH₂ [58]. The absorption band at 2922 cm⁻¹ is from the saturation -C-H asymmetric stretching vibration absorption peak [59]. There is a peak at 1603 cm⁻¹, which belongs to the stretching vibrations of C=O and C=C groups [60]. There is a peak at 1376 cm⁻¹,

which may be caused by the C-H bending vibration of $-\text{CH}_3$ [60]. There is a strong peak at 1272 cm^{-1} and 1071 cm^{-1} , which may be caused by C-O-C stretching vibration [61]. This indicates that EASLE is a potential excellent inhibitor.

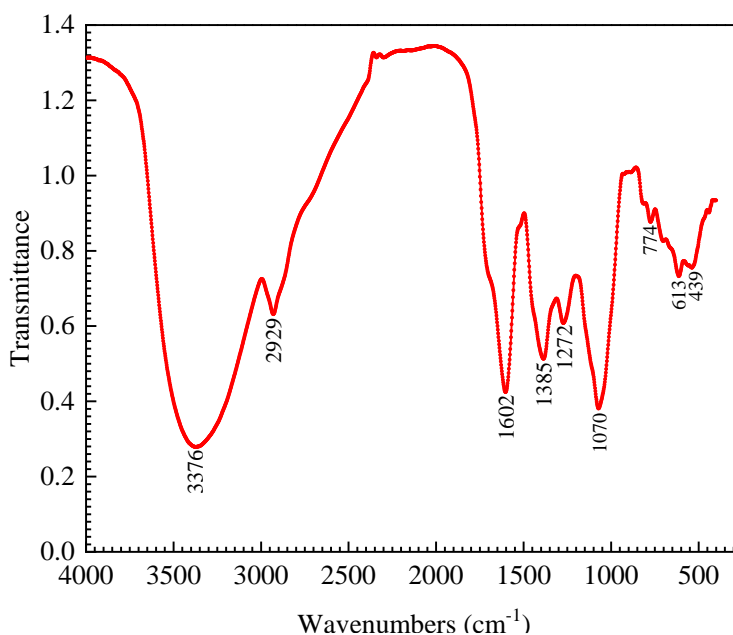


Figure 1. FTIR spectra of EASLE.

3.2. Inhibitory effect of EASLE and adsorption isotherm

There were black corrosion products adhering to the CRS surface after being immersed in uninhibited Cl_3CCOOH solution, indicating that Cl_3CCOOH causes severe corrosion of CRS. The corrosion rate (ν) values of CRS in $0.10\text{ M Cl}_3\text{CCOOH}$ solution are $17.50\text{ g m}^{-2}\text{ h}^{-1}$ (15°C), $19.45\text{ g m}^{-2}\text{ h}^{-1}$ (20°C), $24.88\text{ g m}^{-2}\text{ h}^{-1}$ (25°C) and $32.22\text{ g m}^{-2}\text{ h}^{-1}$ (30°C). With the addition of EASLE, ν is reduced gradually along with the advance of EASLE concentration.

Fig. 2 represents the relationship between η_w and EASLE concentration (c) in $0.10\text{ M Cl}_3\text{CCOOH}$. At all temperatures, η_w continuously increases with the advance of the concentration of EASLE. The higher concentration of EASLE, the more adsorption amount on CRS surface. When the concentration of EASLE exceeds 50 mg L^{-1} , the increasing extent of η_w with c decreases, which may be due to the saturation of EASLE adsorption on CRS surface. As the temperature is increased, η_w decreases to some extent at a certain inhibitor concentration. When the temperature is 15°C , the maximum η_w of 100 mg L^{-1} EASLE is 91.1% . However, when the experimental temperature is up to 30°C , η_w of 100 mg L^{-1} EASLE is reduced to 62.6% . This is because the corrosion of CRS by Cl_3CCOOH is severely accelerated at higher temperature, which accelerates the precipitation rate of H_2 , and then weakens the adsorption of EASLE molecules on the surface of CRS.

A comparison of inhibition efficiency of EASLE with other literature data previously reported on inhibitors for steel in Cl_3CCOOH solution is presented in Table 1. It can be seen from Table 1 that all inhibitors except the individual walnut green husk extract have inhibition efficiency of more than

90%. Although sodium dodecyl sulfate exhibits a high inhibition efficiency, it has a stimulating effect on respiratory tract, harmful to human health, heat decomposition will release irritant toxic gas, and flammable [62]. Therefore, it is not conducive to industrial application. Calcium lignosulfonate, imidazoline, triazolyl blue tetrazolium bromide are of high cost, which limits the widespread application in industry. The inhibition efficiency of walnut green husk extract alone is only 63.4%, while the inhibition efficiency of walnut green husk extract/KI mixture reaches above 90%. It should be noted that the additive compound of KI is still of high cost. By considering comprehensively, EASLE is qualified to be used as an efficient and low-cost inhibitor for CRS corrosion in Cl_3CCOOH medium, which has a good prospect in the field of corrosion inhibitors.

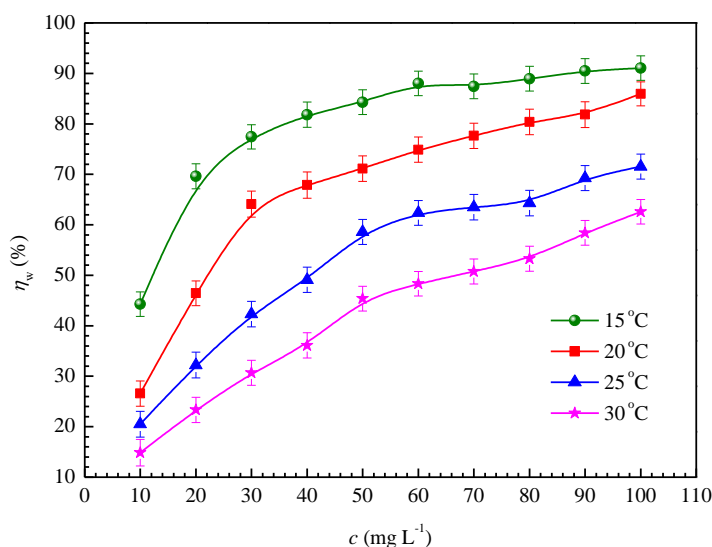


Figure 2. Relationship between inhibition efficiency (η_w) and the concentration of EASLE (c) in 0.10 M Cl_3CCOOH solution.

Table 1. Comparison of inhibition efficiency (η_w) of EASLE with the literature data of previous inhibitors for CRS in 0.10 M Cl_3CCOOH solution

Inhibitor	T ($^{\circ}\text{C}$)	c (inhibitor)	η_w (%)	Ref.
EASLE	20	100 mg L^{-1}	91.1	This paper
calcium lignosulfonate	25	2.0 g L^{-1}	92.9	[45]
sodium dodecyl sulfate	20	50 mg L^{-1}	90.5	[46]
imidazoline	20	500 mg L^{-1}	95.9	[47]
triazolyl blue tetrazolium bromide	25	1.0 mM	95.5	[48]
bamboo leaves extract	20	200 mg L^{-1}	96.1	[49]
walnut green husk extract	20	200 mg L^{-1}	63.4	[50]
walnut green husk extract + KI	20	200 mg L^{-1} + 200 mg L^{-1}	97.2	[50]

In order to better explain the adsorption behavior of EASLE on CRS surface, Langmuir adsorption isotherm as shown in Eq. (5) [63] was used to fit with the experimental data.

$$\frac{c}{\theta} = \frac{1}{K} + c \quad (5)$$

where c is the inhibitor concentration (mg L^{-1}), K is the adsorption equilibrium constant (L mg^{-1}), and θ is the surface coverage with the approximate value of inhibition efficiency (η_w).

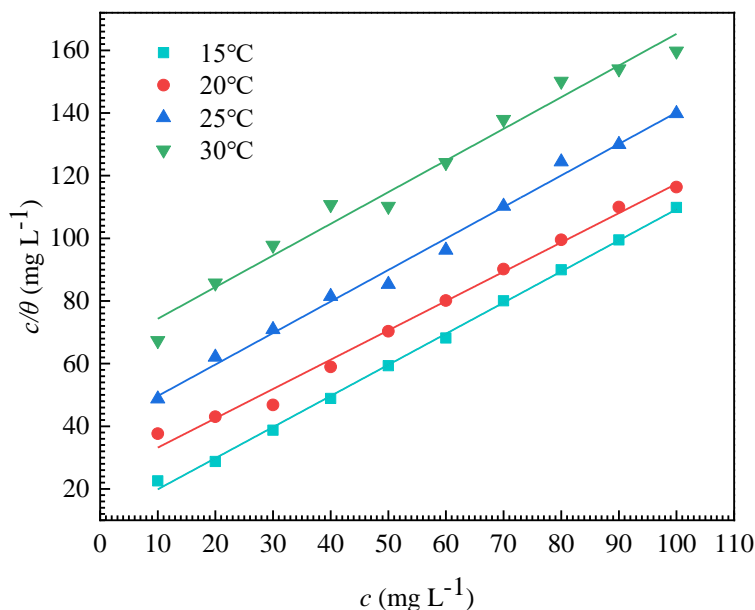


Figure 3. The fitted straight lines of $c/\theta - c$ in 0.10 M Cl_3CCOOH at different temperatures using weight loss method with the immersion time of 6 h.

Table 2. Linear regression parameters between c/θ and c in 0.10 M Cl_3CCOOH solutions at 15 - 30 °C.

T (°C)	r^2	slope	intercept	K (L mg^{-1})
15	0.9984	0.99	9.95	0.10050
20	0.9920	0.94	23.83	0.04196
25	0.9924	1.01	35.60	0.02809
30	0.9784	1.01	64.21	0.01557

Fig. 3 represents the fitted straight lines of $c/\theta - c$ at different temperatures. Table 2 lists their linear regression parameters and corresponding K values. Adsorption isotherm is usually used to evaluate the adsorption capacity of inhibitor on steel surface. The data in Table 2 and Fig. 3 represents that the correlation coefficient (r^2) of all fitted lines of $c/\theta - c$ are very close to 1, which indicates that the adsorption of EASLE on CRS surface follows Langmuir isotherm at all studied temperatures. It is worth noting that the slope values at different temperatures are close to 1, indicating that the interaction force among EASLE molecules adsorbed on CRS surface is negligible. It is generally accepted that the larger K always means the stronger adsorption capacity of inhibitor molecules on metal surface. As also can be seen from Table 2, K reduces with the increase of experimental

temperature. In other words, it is easier for EASLE to adsorb onto CRS/solution interface at lower temperatures. At higher temperatures, the collision turns to be more severely stronger, and the adsorbed EASLE molecules are easy to desorb from CRS surface, resulting in the reduction of inhibition at high temperatures.

3.3. PDP of CRS in Cl_3CCOOH solution

In order to investigate whether cathodic or anodic reaction of CRS electrode is retarded by EASLE, PDP are fully tested. Fig. 4 represents PDP of CRS in 0.10 M Cl_3CCOOH solutions in the absence and presence of different concentrations of EASLE at 15°C. Clearly, the shape of PDP does not change before and after adding EASLE, and so the electrochemical corrosion mechanism of CRS in Cl_3CCOOH solution does not alter. Along with the increase of EASLE concentration, both cathodic and anodic branches move toward the left direction of low corrosion current densities. Comparing with anodic reaction, the cathodic reaction is more efficiently retarded by EASLE. This indicates that EASLE is a mixed inhibitor while mainly retards the cathodic reaction. The linear Tafel region in the cathodic branch is relatively evident. On the contrary, the Tafel interval of the anode polarization curve is difficult to discern. Accordingly, it is rather difficult to obtain the accurate electrochemical corrosion parameters through Tafel extrapolations of both anodic and cathodic branches [64]. Herein, the corrosion parameters are obtained by firstly extending the wide cathodic Tafel lines to around corrosion potential, and then extending the weak anodic polarization region [65]. This fitting method is also of high accuracy, which is well consistent with weight loss measurement [66].

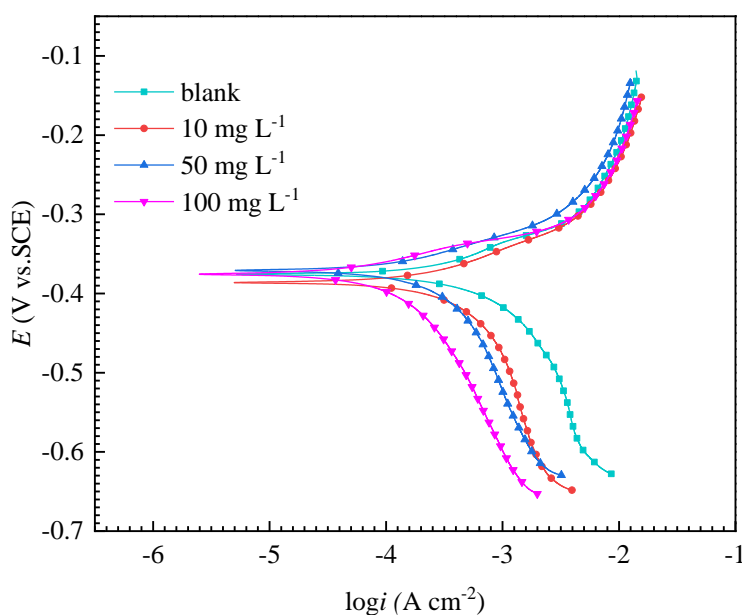


Figure 4. PDP for CRS in 0.10 M Cl_3CCOOH in the absence and presence of different concentrations of EASLE at 15 °C (immersion time is 2 h).

Table 3. PDP parameters for the corrosion of CRS in 0.10 M Cl_3CCOOH containing different concentrations of EASLE at 15°C (immersion time is 2 h)

c (mg L^{-1})	E_{corr} (mV vs. SCE)	i_{corr} ($\mu\text{A cm}^{-2}$)	$-b_c$ (mV dec^{-1})	b_a (mV dec^{-1})	η_p (%)
0	-375 ± 5	1869 ± 9	565 ± 7	193 ± 7	—
10	-386 ± 4	643 ± 7	470 ± 5	99 ± 9	65.6
50	-371 ± 5	346 ± 6	342 ± 5	77 ± 8	81.6
100	-376 ± 4	135 ± 6	231 ± 6	47 ± 8	92.8

The corrosion electrochemical parameters are listed in Table 3. The corrosion potential (E_{corr}) remains unchangeable upon with the addition of the plant inhibitor of EASLE, indicating that the inhibition mechanism of EASLE is through "geometric blocking effect". Prof. Cao [67] in 1996 proposed that "geometric blocking effect" means the inhibition effect comes from the reduction of the reaction area on the surface of the corroding metal. If the inhibition performance is caused by the surface of the adsorbed inhibitor molecules, E_{corr} in uninhibited solution is almost equal to that in inhibited solution, in which case inhibitory efficiency corresponds to the coverage of the adsorbed species. The corrosion current density (i_{corr}) of CRS in the inhibition system decreases more than that in the blank solution in Table 3, and i_{corr} decreases with the increase of EASLE concentration. Tafel slopes of the cathode (b_c) and anode (b_a) decrease with the increase of EASLE concentration, so the cathodic polarization overpotential of the steel electrode in this inhibition system changes with the change of current density. The results show that EASLE effectively suppresses the corrosion of CRS in Cl_3CCOOH solution, and η_p increases with the increase of EASLE concentration. When the concentration of EASLE is 100 mg L^{-1} , the maximum η_p is 92.8%. Thus, EASLE performs efficient inhibition performance on the corrosion of CRS in Cl_3CCOOH solution.

3.4. EIS of CRS in 0.10 M Cl_3CCOOH solution

Fig. 5(a) shows Nyquist plots of the corrosion of CRS in 0.10 M Cl_3CCOOH solutions in the absence and presence of 10, 50 and 100 mg L^{-1} EASLE at 15°C. The Nyquist spectrum consists of a large capacitive loop in the high-frequency region followed by a small inductive section in the low-frequency region. It should be noted that the capacitive loop at high frequencies is not the perfect semicircle, which is mainly due to the dispersion effect that is caused by the nonuniformity of the electrode surface and the nonuniformity of adsorption and diffusion during the corrosion of CRS surface [68]. On the other hand, the small inductive section may be related to the unstable state caused by the adsorption-desorption process of H_3O^+ , Cl_3CCOO^- or inhibitor molecules [69]. It may also be attributed to redissolution of passivated CRS surface at low frequencies [70]. The large capacitive loop at HF mirrors the relaxation process and charge transfer resistance of the boundary layer [71]. The radius of capacitive loop increases with the increase of the concentration of EASLE, indicating that the inhibition of EASLE is gradually enhanced. In addition, Nyquist plot with EASLE is similar to that in

blank solution, and so the electrochemical corrosion mechanism of CRS in Cl_3CCOOH is not altered after adding EASLE.

Fig. 5(b) shows the Bode modulus of the corrosion of CRS in 0.10 M Cl_3CCOOH in the absence and presence of different concentrations of EASLE at 15°C. Along with the advance of EASLE concentration, the absolute bode modulus moves to a higher value in the low-frequency region, confirming that the inhibitive ability of EASLE. This is related to the adsorption of inhibitor molecules on the steel surface [72,73]. The higher the concentration of EASLE, the more adsorption of EASLE molecules on CRS surface, thus increasing the surface coverage [74]. Therefore, the inhibition effect increases with the increase of EASLE concentration. Fig. 5(c) shows Bode phases of the corrosion of CRS in 0.10 M Cl_3CCOOH in the absence and presence of different concentrations of EASLE at 15°C. A distinct phase peak can be clearly seen at the middle frequencies, which corresponds to the capacitance loop in the Nyquist plot. And the phase peak angle advances with the increase of EASLE concentration. Notably, all phase angles are less than 90, indicating a dispersion effect in the test system [74]. This is consistent with the result of Nyquist plots.

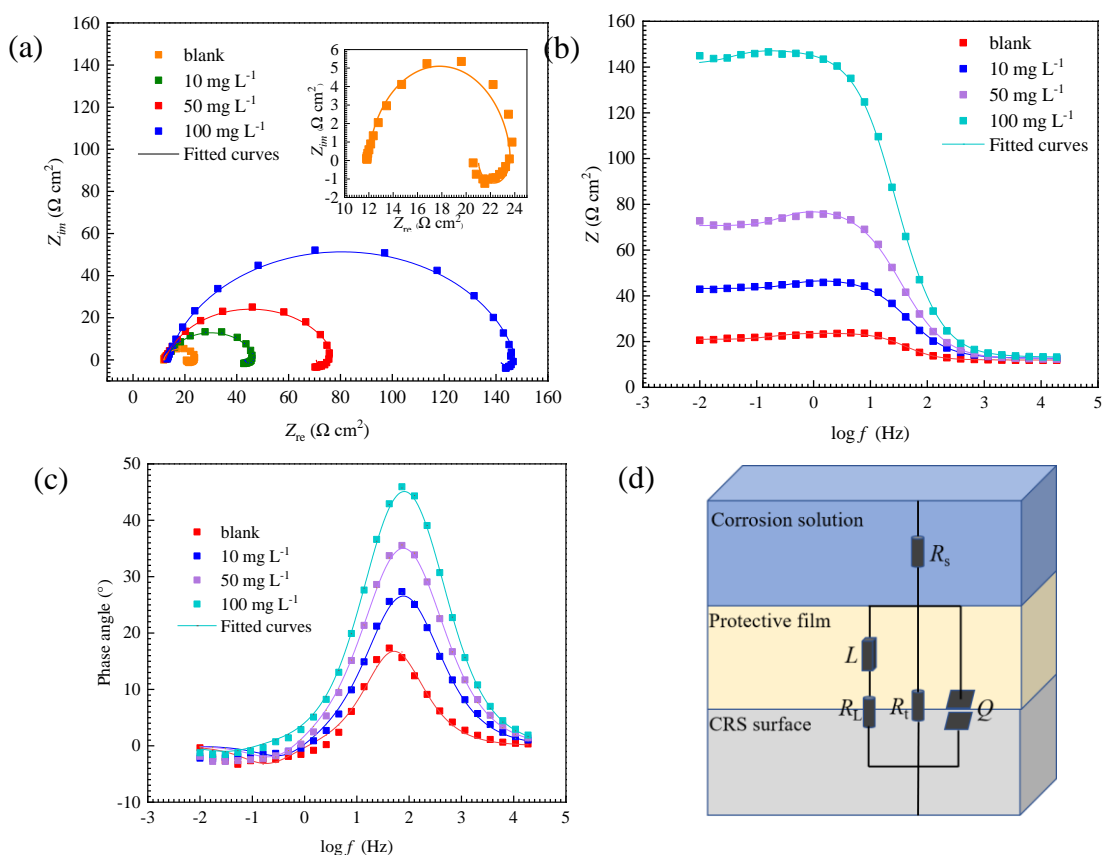


Figure 5. EIS of the corrosion of CRS in 0.10 M Cl_3CCOOH solutions in the absence and presence of different concentrations of EASLE at 15 °C: (a) Nyquist plots; (b) Bode modulus; (c) Bode phases; (d) Equivalent circuit used to fit the EIS.

Table 4. EIS parameters for the corrosion of CRS in 0.10 M Cl₃CCOOH containing different concentrations of EASLE at 15°C (immersion time is 2 h)

<i>c</i> (mg L ⁻¹)	<i>R_s</i> (Ω cm ²)	<i>R_p</i> (Ω cm ²)	<i>R_L</i> (Ω cm ²)	<i>L</i> (H cm ²)	<i>Q</i> (μΩ s ^{<i>n</i>} cm ⁻²)	<i>n</i>	χ ² (10 ⁻⁴)	η _R (%)
0	12.0 ± 0.3	11.8 ± 1.2	39.3 ± 8.5	39 ± 5	543 ± 5	0.9325 ± 0.02	6.1	—
10	12.6 ± 0.4	35.0 ± 1.6	246.0 ± 7.2	106 ± 7	339 ± 7	0.8235 ± 0.02	4.8	66.3
50	12.3 ± 0.3	66.5 ± 1.5	478.9 ± 9.1	294 ± 5	248 ± 6	0.8134 ± 0.02	4.9	82.3
100	13.2 ± 0.3	134.9 ± 1.5	2697 ± 9.8	11780 ± 9	128 ± 6	0.8455 ± 0.02	1.2	91.3

The equivalent circuit diagram as shown in Fig. 5(d) is used to fit the experimental EIS data, and the fitting corrosion parameters are listed in Table 4. The chi-square (χ²) represents the fitting error, and low χ² indicates the low fitted error for the used equivalent circuit. The solution resistance (*R_s*) is very small, which suggests that the solution of 0.10 M Cl₃CCOOH is of good conductivity. The actual impedance difference between lower and higher frequencies is generally considered to be the charge transfer resistance [75]. However, in this region, there are also diffusion layers, adsorbents and the influence of the solution itself, so the contribution of each resistor must be considered [76]. It is the sum of charge transfer resistance (*R_{ct}*), diffusion layer resistance (*R_d*), accumulation resistance (*R_a*), film resistance (*R_f*), that is, polarization resistance (*R_p*) [77]. As the concentration of EASLE increases, the polarization resistance (*R_p*) increases accordingly, indicating that the corrosion process between corrosive medium and CRS interface is efficiently retarded for the inhibited solution. This result is related to the adsorption inhibitive film formed by EASLE on the surface of CRS that hinders the charge transfer. *R_L* represents the inductance resistance. *Q* represents the constant phase element. The decrease of *Q* in inhibited solution confirms that EASLE adsorption on CRS surface, so that water molecules with relatively large dielectric constant are replaced, which may also be attributed to the increase of the thickness of the interface double electric layer [78]. The inductance value (*L*) value is 39.26 H cm² in the blank solution, but it turns to be higher after adding the inhibitor of EASLE. As the additive concentration of EASLE is up to 100 mg L⁻¹, the *L* value reaches as high as 11780 H cm². The results show that H₃O⁺ and Cl₃CCOO⁻ are the main adsorbents on CRS surface in uninhibited solution, while EASLE molecules are the main adsorbents on CRS surface in inhibited solution [78]. The parameter of *n* represents the dispersion effect coefficient, and its value is less than 1, which confirms the existence of frequency dispersion effect at the interface of CRS surface/aggressive solution [79,80]. With the increase of EASLE concentration, the deviation degree of *n* from 1 becomes more evident. It is concluded that the dispersion effect is more evident after adding EASLE. This may be related to the adsorption and desorption of EASLE at the interface of CRS surface and corrosive medium. η_R enhances with the increase of EASLE concentration, and the maximum η_R is 91.3% when the concentration of EASLE is 100 mg L⁻¹, and so EASLE can effectively reduce the corrosion of CRS in Cl₃CCOOH.

Inhibition efficiency values of 100 mg L⁻¹ EASLE are 91.1%, 92.8% and 91.3% for weight loss, potentiodynamic polarization curves and EIS, respectively. Thus, there is a little difference among these three methods.

3.5. SEM morphologies of CRS surfaces

CRS surface morphologies were observed by SEM. As shown in Fig. 6(a), SEM morphology of polished freshly CRS is relatively smooth, and the grinding traces of emery papers can be evidently observed. The smoothness of CRS surface and the marks of emery papers polishing are more obvious at high resolution with 5 μm , as shown in Fig. 6(b). Fig. 6 (c) shows the surface of CRS after immersion in Cl_3CCOOH solution, which is severely corroded with an uneven surface and an absorption layer of corrosion products attached. Increasing the resolution, it can be further seen in Fig. 6(d) that the surface and interior of the CRS are also heavily corroded, and the corrosion products are arranged in layers or ravines. The corrosion degree is significantly dropped after adding EASLE. It can be seen from Fig. 6(e) that the CRS surface is relatively smooth at 20 μm . In Fig. 6(f), this phenomenon can also be observed more clearly, and a layer of attachment can be found on CRS surface at 5 μm . It may be attributed to that EASLE molecules adsorb on CRS surface to form a protective film [81,82], so as to exhibit efficient inhibitive action. Comparing Fig. 6(f) with (d), it can be easily concluded that EASLE acts as an excellent inhibitor to protect CRS surface from Cl_3CCOOH solution.

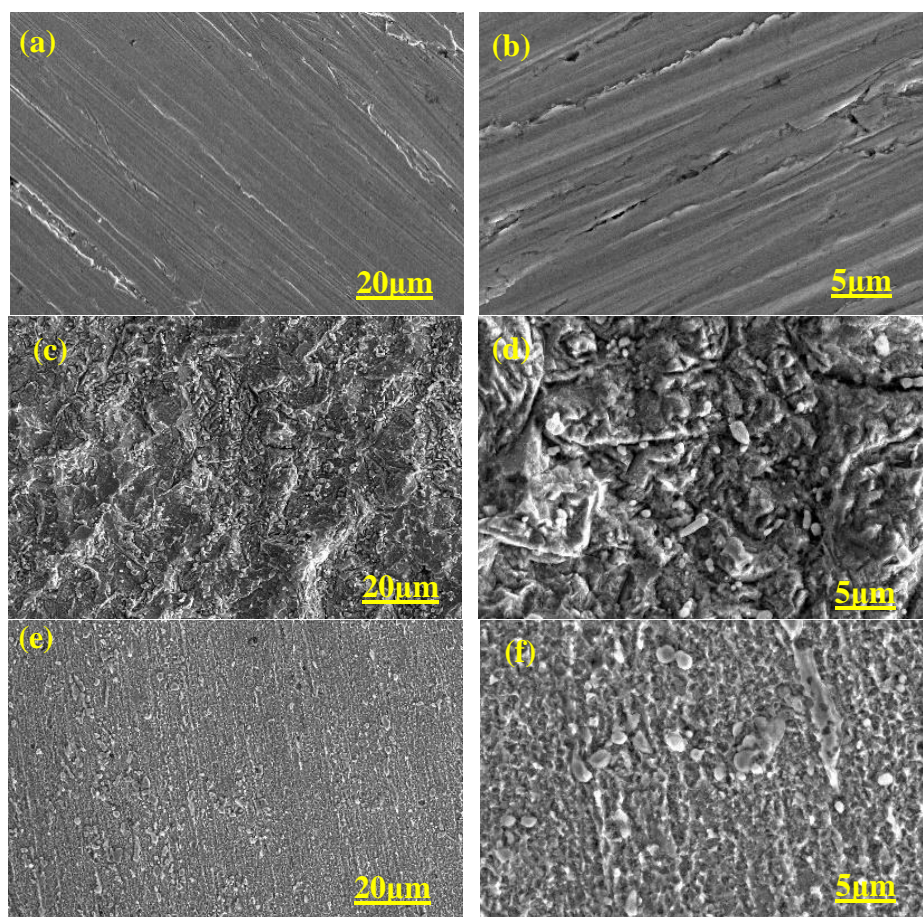


Figure 6. SEM images of CRS surfaces: (a, b) before immersion; (c, d) after 6 h of immersion in 0.10 M Cl_3CCOOH at 15 °C; (e, f) after 6 h of immersion in 100 mg L⁻¹ EASLE + 0.10 M Cl_3CCOOH at 15 °C.

3.6. AFM morphologies of CRS surfaces

The surfaces of CRS are further characterized by AFM so as to deeply observe the micrographs as well as surface roughness. Fig. 7 summarizes 3D-AFM, tapping amplitude and tapping phase images of CRS surfaces. As shown in Fig. 7(a), the surface of the freshly treated CRS is almost flat, but there are still some defects and particles, which can also be clearly observed in Fig. 7(b). These defects and particles are caused by the polishing of emery papers. In Fig. 7(c), there are some white granular materials on the red substrate surface, which may be some carbides in the CRS or oxidized inclusions in the scratches [83]. As shown in Fig. 7(d), the CRS is completely corroded, and its surface becomes rather rough after being immersion in 0.10 M Cl_3CCOOH solution. It can also be seen from Fig. 7(e) that the surface of the CRS is uneven with obvious corrosion marks. In Fig. 7(f), the surface of the CRS is covered with yellow corrosion products, and the matrix cannot be found. Inspection of Fig. 7 (g) reveals that the corrosion degree of CRS surface is greatly reduced after adding EASLE. Comparing with Fig. 7(e), the CRS surface in Fig. 7(h) is relatively smoother. In Fig. 7(i), most of the matrix can be observed, in addition to which a layer of attachment remains. It may be due to the adsorption film of EASLE molecules on the surface of CRS [84-86], so as to play an inhibition effect.

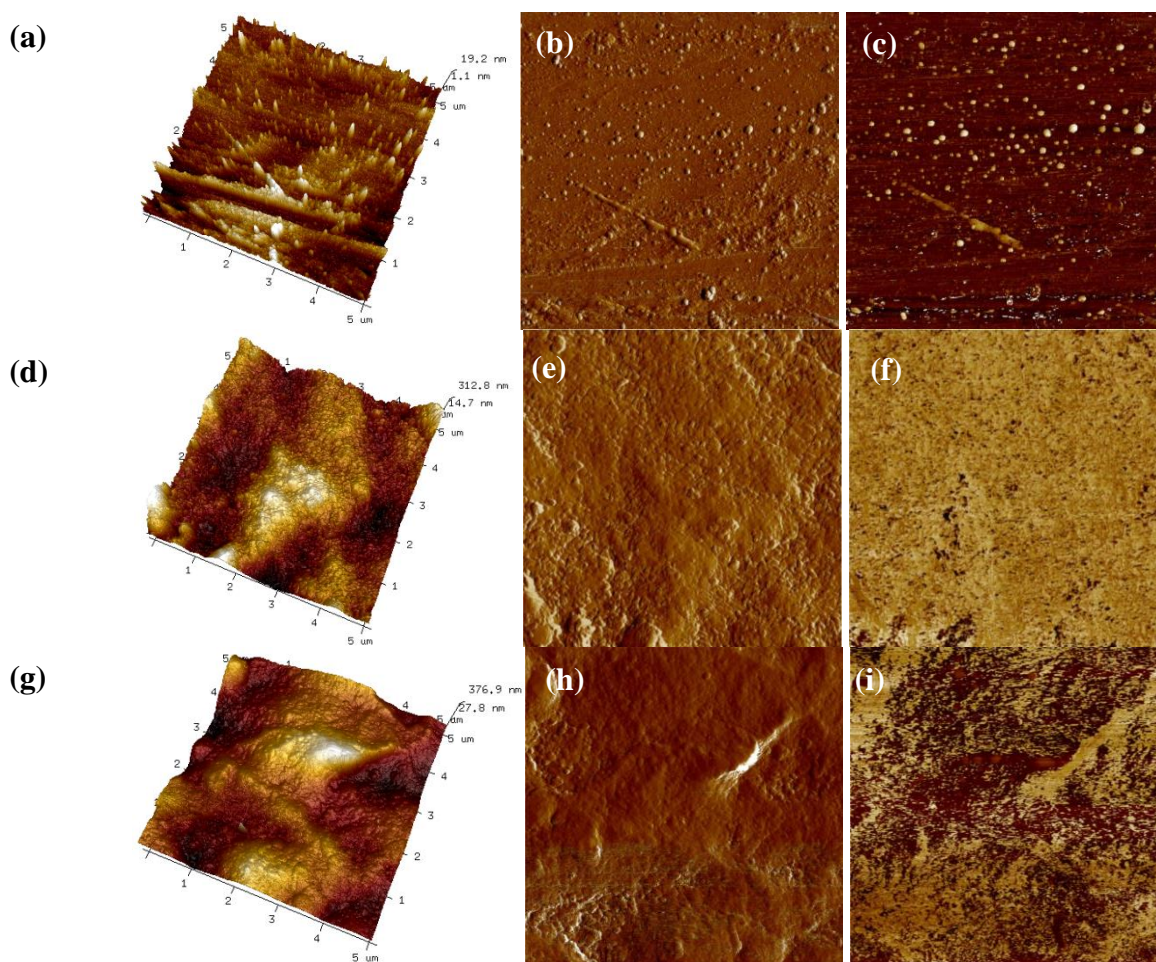


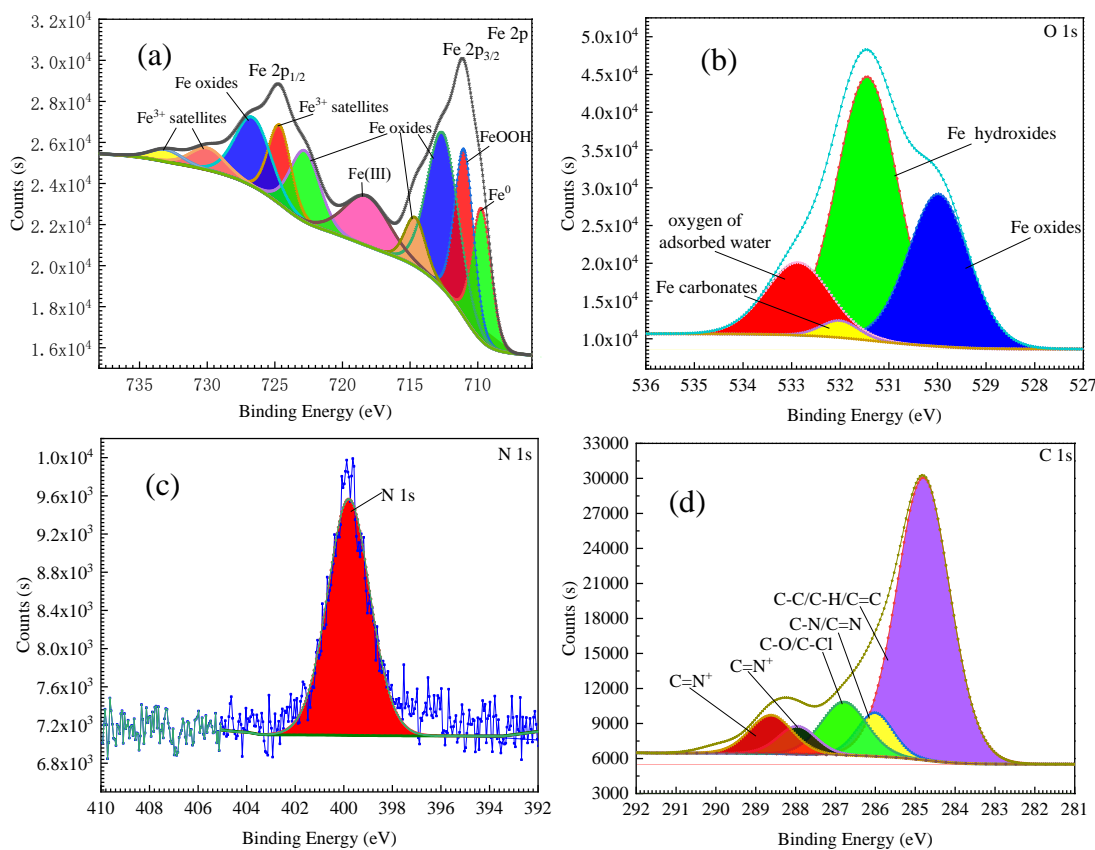
Figure 7. 3D-AFM (a,d,g), tapping amplitude (b,e,h) and tapping phase (c,f,i) images of CRS surfaces: (a-c) before immersion; (d-f) after 6 h of immersion in 0.10 M Cl_3CCOOH at 15 °C; (g-i) after 6 h of immersion in 100 mg L⁻¹ EASLE + 0.10 M Cl_3CCOOH at 15 °C.

Table 5. Surface roughness parameters of AFM images of CRS surfaces before and after 6 h of immersion in 0.10 M Cl_3CCOOH without and with EASLE at 15 °C.

CRS surface	$P-V$ (nm)	R_q (nm)	R_a (nm)
Before immersion	60.3 ± 3.6	4.6 ± 1.2	3.3 ± 0.8
$\text{Cl}_3\text{CCOOH} + \text{CRS}$	622 ± 5.2	85.6 ± 3.2	68.1 ± 1.1
$\text{Cl}_3\text{CCOOH} + \text{EASLE} + \text{CRS}$	668 ± 5.3	93.1 ± 3.9	73.2 ± 1.2

Surface roughness parameters corresponding to AFM micro-images are shown in Table 5. In Table 5, R_a is the average surface roughness, R_q is the mean square roughness, and $P-V$ is the peak-to-valley. All these parameters are the lowest for the polished CRS surface. After immersion in 0.10 M Cl_3CCOOH for 6 h, R_a , R_q and $P-V$ of CRS surfaces are significantly increased, which is attributed to the severe corrosion of the CRS surface. After adding EASLE, R_a , R_q and $P-V$ of the inhibited CRS surface turn to decrease to more extent, which is caused by the adsorption film formed by EASLE molecules on the surface of CRS.

3.7. XPS of inhibited CRS surface by EASLE

**Figure 8.** XPS high-resolution spectrum of CRS after 6 h of immersion at 15 °C in 100 mg L^{-1} EASLE + 0.10 M Cl_3CCOOH : (a) Fe 2p; (b) O 1s; (c) N 1s; (d) C 1s.

In order to further verify the adsorption of EASLE molecules on CRS surface, CRS surface is characterized by XPS. Fig. 8 is XPS high-resolution spectrum of CRS after 6 h of immersion at 20 °C in 0.10 M Cl_3CCOOH solution with 100 mg L^{-1} EASLE. Fe 2p signals contain bimodal properties as a result of multiple spectral splitting due to the presence of unpaired valence electrons [87]. Two distinct peaks can be clearly found in Fig. 8(a), the 711 eV is Fe 2p_{3/2} XPS spectrum and the 724 eV is Fe 2p_{1/2} XPS spectrum. Through further analysis of the two main peaks, Fe 2p_{3/2} spectrum consists of four peaks at 709, 711, 712 and 714 eV, which are assigned to Fe⁰, FeOOH, Fe oxides (Fe₂O₃, Fe₃O₄) [88,89]. Fe 2p_{1/2} spectrum consists of three peaks at 722 eV, 726 eV and 724 eV assigned for Fe oxides (Fe₂O₃, Fe₃O₄) and Fe³⁺ satellites. In addition, 718 eV is considered to be Fe (III), 730 eV and 733 eV are considered to be Fe³⁺ satellites [90]. Fig. 8(b) is O 1s high resolution spectrum. It can be fitted into four main peaks, respectively at 529.9 eV, 531.4 eV, 532.0 eV, 532.9 eV. The peaks of 529.9 eV, 531.4 eV, 532.0 eV may be related to Fe oxides, which comes from O²⁻ (Fe₂O₃, Fe₃O₄), OH⁻ (FeOOH) and Fe carbonates [90,91]. The peak of 532.9 eV may be assigned to oxygen of adsorbed water [92]. The N 1s spectrum as shown in Fig. 12(c), a wide peak can be clearly seen at 400 eV, which comes from C-N bond [92]. Five peaks are obtained by fitting the high-resolution narrow spectrum of C1s in Fig. 12(d). The first peak of 284.8 eV has the major influence and corresponds to C-C, C-H of aromatic bonds and C=C [93]. The second peak at 286 eV is due to C-N or C=N [94]. The third peak at 286.8 eV can be related to C-O, C-N and C-H groups [95]. The fourth and fifth peaks at 288 eV and 288.7 eV may be attributed to C=N⁺ [96,97]. The above results confirm that EASLE efficiently adsorb on CRS surface to achieve inhibition efficiency.

3.8. Inhibition mechanism of EASL

The corrosion of the steel was significantly inhibited by the addition of EASLE to the Cl_3CCOOH solution. Previous studies [98,99] have shown that there are a large number of flavonoids and phenylpropanoids in EAS. Such as patuletin, apigenin, quercetin, caffeic acid, ferulic acid and chlorogenic acid, the molecular formula is shown in Fig. 9. These substances contain a large number of oxygen atoms and heterocycles, which may be the main effective components of corrosion inhibition. Based on the experimental and empirical formula, macroscopic and microscopic research results, the inhibition mechanism of EASLE in Cl_3CCOOH solution is explained as follows: The polar functional groups of these compounds are mainly hydroxyl (-OH) with conjugated structures, which have a lot of lone pair electrons and π electronics, is a good chelating ligand, so it can be vacant d orbitals forming coordination bond with Fe chemical adsorption [100,101]. In addition, EASLE mostly contains N and O unsaturated polar groups. These compounds are protonated by H_3O^+ , and positively charged in the acid solution, while CRS is negatively charged in the Cl_3CCOOH solution due to the adsorption of Cl_3CCOO^- [102]. Therefore, electrostatic attraction is generated between the protonated compounds and negatively charged CRS surface to form an adsorption membrane, achieving the inhibitive action.

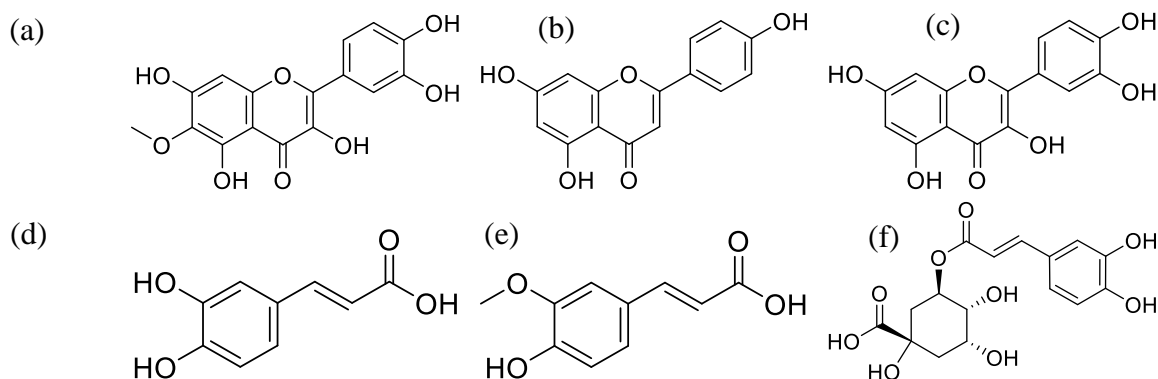


Figure 9. The chemical components in EASSLE: (a) patuletin; (b) apigenin; (c) quercetin; (d) caffeic acid; (e) ferulic acid; (f) chlorogenic acid.

4. CONCLUSION

(1) EASLE represents efficient inhibition effect on CRS in 0.10 M Cl_3CCOOH solution. The inhibition performance enhances with the advance of the concentration of EASLE, while decreases with the advance of temperature. At 15°C and 100 mg L^{-1} , the inhibition efficiency is up to 91.1%. The adsorption of EASLE on CRS surface conforms to Langmuir adsorption isotherm equation. K decreases with the increase of temperature.

(2) After adding EASLE, the corrosion potential of CRS in 0.10 M Cl_3CCOOH medium basically does not change. EASLE is a mixed-type inhibitor whose mechanism is "geometric blocking effect". The Nyquist spectrum mainly presents a single capacitive reactance arc at high frequencies followed by a small inductive section at low frequencies. The charge transfer resistance increases significantly with the addition of EASLE, but the constant phase element decreases to some extent.

(3) The microstructure of SEM and AFM shows that EASLE can effectively inhibit the corrosion degree of steel surface. After the addition of EASLE, the surface roughness of AFM image increases, which is caused by the adsorption film formed by EASLE molecules on CRS surface. The functional groups characterized by XPS also provide strong evidence for the adsorption inhibitor of EASLE on CRS surface.

ACKNOWLEDGEMENTS

Funding support from National Natural Science Foundation of China (52161016, 51761036), Fundamental Research Project for Distinguished Young Scholars in Yunnan Province (202001AV070008), Special Project of "Top Young Talents" of Yunnan Ten Thousand Talents Plan (51900109) and Special Project of "Leading Talents of Industrial Technology" of Yunnan Ten Thousand Talents Plan (80201408) are acknowledged.

References

1. B.R. Hou, X.G. Li, X.M. Ma, C.W. Du, D.W. Zhang, M. Zheng, W.C. Xu, D.Z. Lu, F.B. Ma, *npj Mater. Degrad.*, 1 (2017) 4.
2. J.Y. Hu, D.B. Huang, G.A. Zhang, G.L. Song, X.P. Guo, *Corros. Sci.*, 63 (2012) 367.

3. N. Chaubey, Savita, A. Qurashi, D.S. Chauhan, M.A. Quraishi, *J. Mol. Liq.*, 321 (2021) 114385.
4. P.B. Raja, M. Ismail, S. Ghoreishiamiri, J. Mirza, M.C. Ismail, S. Kakooei, A.A. Rahim, *Chem. Eng. Commun.*, 203 (9) (2016) 1145.
5. S. Mo, H. Q. Luo, N. B. Li, *Chem. Pap.*, 70 (2016) 1131.
6. P.B. Raja, M.G. Sethuraman, *Mater. Lett.*, 62 (17-18) (2008) 2977.
7. A. Ostovari, S.M. Hoseinie, M. Peikari, S.R. Shadizadeh, S.J. Hashemi, *Corros. Sci.*, 51 (9) (2009) 1935.
8. A.Y. El-Etre, M. Abdallah, Z.E. El-Tantawy, *Corros. Sci.*, 47 (2) (2005) 385.
9. A.K. Satapathy, G. Gunasekaran, S.C. Sahoo, K. Amit, P.V. Rodrigues, *Corros. Sci.*, 51 (12) (2009) 2848.
10. P.B. Raja, M.G. Sethuraman, *Mater. Corros.*, 60 (2009) 22.
11. P. Kalaiselvi, S. Chellammal, S. Palanichamy, G. Subramanian, *Mater. Chem. Phys.*, 120 (2-3) (2010) 643.
12. S. Garai, S. Garai, P. Jaisankar, J.K. Singh, A. Elango, *Corros. Sci.*, 60 (2012) 193.
13. M. Behpour, S.M. Ghoreishi, M. Khayatkashani, N. Soltani, *Mater. Chem. Phys.*, 131 (3) (2012) 621.
14. P.B. Raja, A.K. Qureshi, A.A. Rahim, H. Osman, K. Awang, *Corros. Sci.*, 69 (2013) 292.
15. E. Ituen, A. James, O. Akaranta, S. Sun, *Chin. J. Chem. Eng.*, 24 (10) (2016) 1442.
16. A. Ehsani, M.G. Mahjani, M. Hosseini, R. Safari, R. Moshrefi, H.M. Shiri, *J. Colloid Interf. Sci.*, 490 (2017) 444.
17. R. Haldhar, D. Prasad, A. Saxena, *J. Environ. Chem. Eng.*, 6 (2) (2018) 2290.
18. V.V. Torres, R.S. Amado, C.F. Sá, T.L. Fernandez, C.A.S. Riehl, A.G. Torres, E. D'Elia, *Corros. Sci.*, 53 (7) (2011) 2385.
19. M. Faustini, A. Maciuk, P. Salvin, C. Roos, M. Lebrini, *Corros. Sci.*, 92 (2015) 287.
20. A.M. Abdel-Gaber, B.A.A. Nabey, I.M. Sidahmed, A.M. El-Zayady, M. Saadawy, *Corrosion*, 62 (4) (2006) 293-299.
21. J.C. Rocha, J.A.C.P. Gomes, E. D'Elia, *Corros. Sci.*, 52 (7) (2010) 2341.
22. U.F. Ekanem, S.A. Umoren, I.I. Udousoro, A.P. Udoh, *J. Mater. Sci.*, 45 (2010) 5558.
23. G. Ji, S. Anjum, S. Sundaram, R. Prakash, *Corros. Sci.*, 90 (2015) 107.
24. K.O. Orubite, N.C. Oforka, *Mater. Lett.*, 58 (11) (2004) 1768.
25. P. Mourya, S. Banerjee, M. M. Singh, *Corros. Sci.*, 85 (2014) 352.
26. E.E. Oguzie, *Corros. Sci.*, 50 (11) (2008) 2993.
27. E.E. Oguzie, *Mater. Chem. Phys.*, 99 (2-3) (2006) 441.
28. R.P. Bothi, R.A. Abdul, O. Hasnah, A. Khalijah, *Acta Phys.-Chim. Sin.*, 26 (2010) 2171.
29. L.R. Chuanhan, G. Gunasekaran, *Corros. Sci.*, 49 (3) (2007) 1143.
30. S.H. Zaferani, M. Sharifi, D. Zaarei, M.R. Shishesaz, *J. Environ. Chem. Eng.*, 1 (4) (2013) 652.
31. M. Goyal, S. Kuma, I. Bahadur, C. Verma, E.E. Ebenso, *J. Mol. Liq.*, 256 (2018) 565.
32. A.Y. El-Etre, *Appl. Surf. Sci.*, 252 (2006) 8521.
33. B.E.A. Rani, B.B.J. Basu, *Int. J. Corros.*, 2012 (2012) 1.
34. X.H. Li, S.D. Deng, H. Fu, X.G. Xie, *Corros. Sci.*, 78 (2014) 29.
35. X.H. Li, S.D. Deng, H. Fu, *Corros. Sci.*, 62 (2012) 163.
36. X.H. Li, S.D. Deng, H. Fu, *J. Appl. Electrochem.*, 40 (2010) 1641.
37. M. Tang, X.H. Li, S.D. Deng, R. Lei, *J. Mol. Liq.*, 344 (2021) 117926.
38. X.H. Li, S.D. Deng, G.B. Du, X.G. Xie, *J. Taiwan Ins. Chem. Eng.*, 114 (2020) 252.
39. X.H. Li, S.D. Deng, *Corros. Sci.*, 55 (2012) 407.
40. S.S. Sampat, J.C. Vora, *Corros. Sci.*, 14 (1974) 591.
41. R.T. Vashi, P.S. Desai, *Bull. Electrochem.*, 23 (2007) 87.
42. P.S. Desai, R.T. Vashi, *Indian J. Chem. Technol.*, 17 (2010) 50.
43. P.S. Desai, R.T. Vashi, *Anti-Corros. Meth. Mater.*, 58 (2011) 70.
44. E.E. Ebenso, P.C. Okafor, U.J. Ekpe, *Anti-Corros. Meth. Mater.*, 50 (2003) 414.

45. L.Z. Wang, M. Huang, X.H. Li, *Appl. Chem. Ind.*, 49 (11) (2020) 2711.
46. L.Z. Wang, M. Huang, X.H. Li, *Mater. Prot.*, 54 (08) (2021) 79.
47. L.Z. Wang, X.H. Li, *J. Chin. Soc. Corros. Prot.*, 41 (3) (2021) 353.
48. X.H. Li, S.D. Deng, T. Lin, X.G. Xie, X. Xu, *J. Mol. Liq.*, 274 (2019) 77.
49. X.H. Li, S.D. Deng, N. Li, X.G. Xie, *J. Mater. Res. Technol.*, 6 (2) (2017) 158.
50. X.H. Li, S.D. Deng, *J. Mater. Res. Technol.*, 9 (6) (2020) 15604.
51. M. Kumar, A.K. Verma, S.C. Garkoti, *India. Acta Oecol.*, 109 (2020) 103642.
52. L. Chen, J. Zhou, T. Zeng, Y.F. Miao, L. Mei, G.B. Yao, K. Fang, X.F. Dong, T. Sha, M.Z. Yang, T. Li, Z.W. Zhao, H.B. Zhang, *New Phytol.*, 227 (5) (2020) 1493.
53. R. Wang, J.F. Wang, Z.J. Qiu, B. Meng, F.H. Wan, Y.Z. Wang, *New Phytol.*, 191 (2011) 828.
54. Y.Y. Sun, Q.X. Zhang, Y.P. Zhao, Y.H. Diao, F.R. Gui, G.Q. Yang, *J. Integr. Agric.*, 20 (5) (2021) 1327.
55. P.Y. Liu, D. Liu, W.H. Li, T. Zhao, F. Sauriol, Y.C. Gu, Q.W. Shi, M.L. Zhang, *Chem. Biodiversity*, 12 (10) (2015) 1481.
56. Y.Q. Zhu, Q.Q. Sun, Y. Wang, J. Tang, Y.Y. Wang, H. Wang, *Corros. Sci.*, 185 (2021) 109414.
57. E.A. Noor, *Mater. Chem. Phys.*, 114 (2009) 533.
58. N. Yunitasari, R.T. Swasono, H.D. Pranowo, T.J. Raharjo, *J. Saudi Chem. Soc.*, 26 (2022) 101540.
59. A. Agirre, M. Aguirre, J.R. Leiza, *Polym.*, 253 (2022) 124997.
60. G. Beltrame, I. Mattsson, P. Damlin, Z.H. Han, C. Kvarnström, R. Leino, B. Yang, *J. Mol. Struct.*, 1264 (2022) 133226.
61. Q. Shen, Y.H. Zhang, Y.J. Fan, Z.H. Xu, Z.X. Su, *Trans. Nonferrous Met. Soc. China*, 32 (2022) 2370.
62. M.P. John, K. Zbigniew, T.S. Walter, *J. Agrlc. Food Chem.*, 32 (1904) 782.
63. Q.H. Zhang, B.S. Hou, Y.Y. Li, Y. Lei, X. Wang, H.F. Liu, G.A. Zhang, *Corros. Sci.*, 189 (2021) 109596.
64. F. Mansfeld, *Corros. Sci.*, 47 (2005) 3178.
65. M.A. Amin, S.S. Abd El Rehim, H.T.M. Abdel-Fatah, *Corros. Sci.*, 51 (2009) 882.
66. M.A. Amin, K.F. Khaled, S.A. Fadel-Allah, *Corros. Sci.*, 52 (2010) 140.
67. C. Cao, *Corros. Sci.*, 38 (12) (1996) 2073.
68. K. Zhang, J.M. Lu, J. Li, D.Q. Zhang, L.X. Gao, Y.J. Wang, *Chem. Eng. J.*, 385 (2020) 123406.
69. B. Xu, W.Z. Yang, Y. Liu, *Corros. Sci.*, 78 (2014) 260.
70. A.K. Singh, M.A. Quraishi, *Corros. Sci.*, 52 (2010) 152.
71. A. Salmasifar, M. Edraki, E. Alibakhshi, B. Ramezanzadeh, G. Bahlakeh, *J. Mol. Liq.*, 327 (2021) 114856.
72. K.R. Ansari, M.A. Quraishi, *J. Taiwan Inst. Chem. Eng.*, 54 (2015) 145.
73. L. Guo, B.C. Tan, W.P. Li, Q.B. Li, X. W. Zheng, I.B. Obot, *J. Mol. Liq.*, 327 (2021) 114828.
74. Q.H. Zhang, B.S. Hou, Y.Y. Li, G.Y. Zhu, H.F. Liu, G.A. Zhang, *Corros. Sci.*, 164 (2020) 108346.
75. R. Solmaz, *Corros. Sci.*, 52 (2010) 3321.
76. M. Ozcan, I. Dehri, M. Erbil, *Appl. Surf. Sci.*, 236 (2004) 155.
77. R. Solmaza, G. Kardas, M. Culha, B. Yazici, M. Erbil, *Electrochim. Acta*, 53 (2008) 5941.
78. M.A. Amin, S.S.A. El-Rehim, R.S. Bayoumi, *Electrochim. Acta.*, 52 (11) (2007) 3588.
79. A. Singh, K.R. Ansari, D.S. Chauhan, M.A. Quraishi, H. Lgaz, I.M. Chung, *J. Colloid Interface Sci.*, 560 (2020) 225.
80. F. Zhang, X.H. Li, S.D. Deng, M. Tang, G.B. Du, *J. Mater. Res. Technol.*, 15 (2021) 7050.
81. D.T. Oyekunle, T.I. Oguntade, C.S. Ita, T. Ojo, O.D. Orodu, *Mater. Today Commun.*, 21 (2019) 100691.
82. V. Hemapriya, M. Prabakaran, K. Parameswari, S. Chitra, S.H. Kim, I.M. Chung, *Anti-Corros. Methods Mater.*, 64 (3) (2017) 306.
83. M. Tang, X.H. Li, S.D. Deng, R. Lei, *J. Mol. Liq.*, 334 (2021) 117926.
84. M.A. Bidi, M. Azadi, M. Rassouli, *Mater. Today Commun.*, 24 (2020) 100996.

85. I.M. Chung, R. Malathy, S.H. Kim, K. Kalaiselvi, M. Prabakaran, M. Gopiraman, *J. Adhes. Sci. Technol.*, 34 (14) (2020) 1483.
86. S. Chitra, I.M. Chung, S.H. Kim, M. Prabakaran, *Pigm. Resin. Technol.*, 48 (2019) 389.
87. N.Z.N. Hashima, E.H. Anouarb, K. Kassimcd, H.M. Zakic, A.I. Alharthib, Z. Embonge, *Appl. Surf. Sci.*, 476 (2019) 861.
88. R. Devaux, D. Vouagner, A.M.D. Becdelievre, C. Duret-Thual, *Corros. Sci.*, 36 (1) (1993) 171.
89. P.K. Paul, M. Yadav, *J. Electroanal. Chem.*, 877 (2020) 114599.
90. M. Tourabi, K. Nohair, M. Traisnel, C. Jama, F. Bentiss, *Corros. Sci.*, 75 (2013) 123.
91. W. Temesghen, P.M.A. Sherwood, *Anal. Bioanal. Chem.*, 373 (2002) 601.
92. K.B. Samardzija, C. Lupu, N. Hackerman, A.R. Barron, A. Luttge, *Langmuir*, 21 (26) (2005) 12187.
93. H. Li, S.T. Zhang, B.C. Tan, Y.J. Qiang, W.P. Li, S.J. Chen, L. Guo, *J. Mol. Liq.*, 305 (2020) 112789.
94. O.M.A. Khamaysa, I. Selatnia, H. Zeghache, H. Lgaz, A. Sid, I. Chung, M. Benahmed, N. Gherraf, P. Mosset, *J. Mol. Liq.*, 315 (2020) 113805.
95. M. Bouanisa, M. Tourabia, A. Nyassia, A. Zarroukb, C. Jamac, F. Bentiss, *Appl. Surf. Sci.*, 389 (2016) 952.
96. F.H. Zaidona, K. Kassima, H.M. Zakia, Z. Embongc, E.H. Anouard, N.Z.N. Hashim, *J. Mol. Liq.*, 329 (2021) 115553.
97. A. Singh, K.R. Ansaric, A. Kumard, W.Y. Liu, S.S. Chen, Y.H. Lin, *J. Alloys Compd.*, 712 (2017) 121.
98. Y.Z. Li, R. Zhang, J. Hao, L. Chen, J.Q. Yuan, X.Z. Yang, *J. Chin. Med. Mater.*, 42 (9) (2019) 2058.
99. M. Zhang, W.I. Liu, X. Gao, J.W. Tan, F.H. Wan, *J. Trop. Subtrop. Bot.*, 23 (6) (2015) 697.
100. R.X. Zhao, W.D. Xu, Q. Yu, L. Niu, *J. Mol. Liq.*, 318 (2020) 114322.
101. L.O. Olasunkanmi, A.O. Idris, A.H. Adewole, O.O. Wahab, E.E. Ebenso, *Surf. Interf.*, 21 (2020) 100782.
102. H.M. Elabbasy, H.S. Gadov, *J. Mol. Liq.*, 321 (2021) 114918.